Design, Synthesis, and Biological Assessment of Novel Imidazole and 1,2-Disubstituted Imidazole Derivatives as Potent Antimicrobial Agents

Rashmi Devi[1], Geetanjali[2], Lovely[3], Komal Sharma[4], Neha Yadav[5], Sunena[6*]

[1]Advanced Institute of Pharmacy, Palwal Aurangabad Rashmitewatia3374@gmail.com
[2]Advanced Institute of Pharmacy, Palwal Aurangabad gmahlawat2001@gmail.com
[3]Advanced Institute of. Pharmacy, Palwal Aurangabad aiprawat01@gmail.com
[4]B.S Anangpuria school of pharmaceutical sciences, Alampur, Faridabad komalsharma46622@gmail.com
[5]B.M college of Pharmacy, Farukhnagar nehayadav06398@gmail.com
[6*]Om sterling global University, Hisar
Corresponding Author: Dr. Sunena
Om sterling global University, Hisar

Abstract
The escalating threat of microbial resistance necessitates the continuous design and discovery of novel therapeutic scaffolds. In this study, a diverse library of novel 2,4-disubstituted and 1,2,4-trisubstituted imidazole derivatives was rationally designed, synthesized via multicomponent cyclization, and rigorously characterized using FT-IR, ^{1}H-NMR, mass spectrometry, and elemental microanalysis. The synthesized compounds were systematically evaluated for their *in vitro* antibacterial and antifungal efficacies against a comprehensive panel of pathogenic strains using the agar cup-plate diffusion method. Ciprofloxacin and Fluconazole were utilized as standard therapeutic references. Structure-Activity Relationship (SAR) mapping, coupled with physicochemical assessments (C log P and Molar Refractivity), demonstrated a direct correlation between structural lipophilicity and antimicrobial potency. Notably, the 1,2,4-trisubstituted (N-phenylated) imidazoles exhibited superior broad-spectrum biological activity compared to their 1*H*-imidazole analogs, an effect attributed to optimal steric shielding and enhanced cellular membrane permeation. Structural modifications incorporating electron-donating moieties (*para*-OH, *para*-OCH_3) and lipophilic halogens (*meta*/*para*-Cl) on the C-2 phenyl ring significantly amplified the pharmacological efficacy. Among the screened library, compounds 3d, 3f, 3iv, 3x, 4vi, and 4x emerged as highly potent antimicrobial agents. Specifically, compound 3d [4-(4-(4-chlorophenyl)-1-phenyl-1*H*-imidazol-2-yl)phenol] displayed exceptional, targeted inhibitory activity against the Gram-negative bacterium *Escherichia coli* and the opportunistic fungal mold *Aspergillus flavus*, closely rivaling the standard drugs at equivalent concentrations. These robust *in vitro* findings establish the functionalized tri-substituted imidazole nucleus as a highly promising and optimizable pharmacophore for the development of next-generation antimicrobial therapeutics.

Keywords: Imidazole derivatives; Multicomponent synthesis; Antimicrobial activity; Antifungal activity; Structure-Activity Relationship (SAR); Lipophilicity.
How to cite this article: Devi R, Geetanjali, Lovely, Sharma K, Yadav N, Sunena. Design, Synthesis, and Biological Assessment of Novel Imidazole and 1,2-Disubstituted Imidazole Derivatives as Potent Antimicrobial Agents. Int J Drug Deliv Technol. 2026;16(66s):576-590. DOI: 10.25258/ijddt.16.66s.55

1. Introduction

Heterocyclic compounds, particularly those containing the five-membered planar diazole ring known as imidazole, hold profound clinical significance in contemporary medicinal chemistry and pharmaceutical sciences (Siwach & Verma, 2021). The imidazole nucleus is an integral, naturally occurring pharmacophore present in essential biological molecules, such as the amino acid histidine, the neurotransmitter histamine, and various purine bases, making it a highly compatible structural scaffold for interacting with human biological systems (Verma et al., 2013). Chemically, the imidazole ring contains two nitrogen atoms: a pyrrole-type nitrogen that acts as a hydrogen bond donor and a pyridine-type nitrogen that functions as a hydrogen bond acceptor (Kabir & Uzzaman, 2022). This amphoteric nature and unique electronic configuration enable the imidazole moiety to engage in high-affinity, reversible interactions via hydrogen bonding, pi-pi stacking, and van der Waals forces with diverse biological targets, including critical microbial enzymes and cellular receptors (Yadav & Jain, 2025). Commercially successful and life-saving therapeutics, ranging from the antihistamine clemizole to the proton pump inhibitor omeprazole and the broad-spectrum antifungal agent ketoconazole, heavily underscore the therapeutic versatility of this heterocyclic core (Siwach & Verma, 2021). In recent years, the rapid emergence of multidrug-resistant (MDR) pathogens has triggered a global healthcare crisis, rendering many

conventional antibiotics obsolete. Consequently, imidazole derivatives have become a primary focal point in combating antimicrobial resistance (Al-Ghamdi et al., 2024). These compounds act through multi-targeted mechanisms, such as disrupting microbial cell membrane integrity by inhibiting sterol biosynthesis, interfering with essential DNA replication enzymes like DNA gyrase, and effectively bypassing the efflux pump mechanisms that pathogenic bacteria and fungi deploy to survive traditional pharmacological interventions (Al-Ghamdi et al., 2024; Yadav & Jain, 2025). The rational design of novel, biologically active imidazole derivatives relies heavily on establishing rigorous structure-activity relationships (SAR) through strategic and predictive molecular substitutions on the parent ring (Devi et al., 2024). Modifying the imidazole nucleus at specific positions (primarily C-2, C-4, C-5, and N-1) with varied electron-withdrawing or electron-donating groups significantly alters the overall molecule's pharmacokinetic profile, lipophilicity, molar refractivity (MR), and specific target binding affinity (Rulhania et al., 2021). The lipophilicity of a compound, often expressed as the octanol/water partition coefficient (C log P), is a crucial physical property governing passive membrane partitioning; increasing the partition coefficient typically enhances the molecule's permeability across lipid-rich biological barriers (Lakshmidevi et al., 2024). For instance, the incorporation of highly lipophilic and electron-withdrawing halogen atoms, such as chloro or fluoro groups, at the *para* or *meta* positions of appended phenyl rings profoundly enhances cellular penetration into dense Gram-positive bacterial cell walls and robust fungal cell membranes (Lakshmidevi et al., 2024; Muheyuddeen et al., 2024). Furthermore, introducing bulky aromatic moieties like biphenyl groups or utilizing N-phenylation (substituting the N-1 position with a phenyl ring) to create tri-substituted imidazoles provides critical steric shielding, which increases metabolic stability and restricts the molecule to conformations that optimally fit into the hydrophobic pockets of microbial target enzymes (Pervaiz et al., 2020). Conversely, introducing electron-donating elements such as hydroxyl (-OH) or methoxy (-OCH3) substituents modulates the electronic distribution and augments the hydrogen-bonding capacity of the molecule, an attribute critical for inducing target-specific enzyme inhibition and anchoring the drug to its designated microbial receptor (Muheyuddeen et al., 2024). These targeted chemical substitutions are deliberately selected to optimize the biodistribution profile, augment intrinsic antimicrobial potency, and structurally overcome the defensive resistance mechanisms of modern pathogenic strains (Rulhania et al., 2021). Driven by the escalating global health threat posed by multidrug-resistant pathogens and the continuous demand for safer, highly potent chemotherapeutic agents, the primary objective of this research is to strategically design, synthesize, and evaluate new series of highly functionalized imidazole derivatives. Specifically, this study aims to explore the synthesis of diverse libraries of 2,4-disubstituted and 1,2,4-trisubstituted imidazole architectures utilizing multi-step, cost-effective condensation protocols. The synthetic strategy involves the transformation of starting materials such as 1-(4-chlorophenyl)ethanone and 1-(biphenyl-4-yl)ethanone into corresponding oxoacetaldehydes, followed by cyclization with various substituted benzaldehydes and ammonium acetate. Subsequent N-phenylation will be executed to generate the final tri-substituted target compounds. A critical objective is to confirm the structural integrity and purity of all newly synthesized derivatives using modern analytical and spectral techniques, including Fourier-transform infrared spectroscopy (FT-IR), Proton Nuclear Magnetic Resonance (1H-NMR), Carbon-13 Nuclear Magnetic Resonance (13C-NMR), and high-resolution mass spectrometry. Finally, the synthesized compounds will be subjected to comprehensive *in vitro* biological screening to determine their minimal inhibitory concentrations and zone of inhibition metrics. This biological assessment will be conducted against a broad spectrum of clinically relevant microbial strains, encompassing Gram-positive bacteria, Gram-negative bacteria, and pathogenic fungi, to identify the most potent, safe, and viable lead candidates for future antimicrobial drug development.

2. Experimental Section

2.1. Materials and Instruments

All analytical-grade chemicals were procured from E. Merck and S.D. Fine Chem Ltd., and specific solvents were rigorously purified using conventional distillation methods prior to use. Structural characterizations of the synthesized derivatives were performed using a Shimadzu FT-IR 8400S spectrometer (KBr pellet method), while elemental compositions were accurately verified via a Vario EL III CHNOS analyzer. Nuclear magnetic resonance spectra were systematically recorded on Bruker 300 MHz and 400 MHz NMR spectrometers utilizing DMSO-d6 or $CDCl_3$ as solvents. Finally, precise mass spectrometric analyses were executed on a UPLC-MS/MS system, and all melting points were determined utilizing uncorrected open capillary methods.

2. Experimental Section

2.2. General Synthetic Procedures

2.2.1. Synthesis of Intermediates: The synthetic pathway initiated with the preparation of α-oxoacetaldehyde intermediates via selenium dioxide-mediated oxidation of the corresponding acetophenones. Specifically, 1-(4-

chlorophenyl)ethanone and 1-(biphenyl-4-yl)ethanone were oxidized to yield 2-(4-chlorophenyl)-2-oxoacetaldehyde and 2-(biphenyl-4-yl)-2-oxoacetaldehyde, respectively. This oxidation is essential as it functionalizes the methyl ketone into a 1,2-dicarbonyl system, which subsequently serves as the highly reactive bis-electrophilic partner necessary for the downstream multi-component ring construction (Chen et al., 2013).

2.2.2. Synthesis of 1H-imidazole derivatives (Scheme 1 & 2): The cyclization step utilized a multicomponent Debus-Radziszewski-type reaction to construct the 1H-imidazole ring core. The synthesized 1,2-dicarbonyl intermediates were reacted with various substituted benzaldehydes in the presence of an excess of ammonium acetate, which acts as the bifunctional nitrogen source. Utilizing glacial acetic acid as both the solvent and an acid catalyst under reflux conditions facilitates the formation of an iminium intermediate from the aldehyde, followed by cyclocondensation to yield the di-substituted 4-(4-chlorophenyl)-2-(substituted) phenyl-1H-imidazole (2a-j) and 4-(biphenyl-4-yl)-2-(substituted phenyl)-1H-imidazole (3i-xii) scaffolds (Chen et al., 2013).

2.2.3. Synthesis of 1,2-disubstituted-1H-imidazoles (Scheme 1 & 3): To generate the final fully substituted architectures, the secondary amine (N1 position) of the synthesized 1H-imidazoles was functionalized via an Ullmann-type N-arylation cross-coupling reaction. The 1H-imidazole precursors (2a-j and 3i-xii) reacted with chlorobenzene in tetrahydrofuran (THF), utilizing a mild base (triethylamine) to facilitate the deprotonation of the imidazole nitrogen. This subsequent nucleophilic aromatic substitution-type N-phenylation selectively targets the sterically accessible pyrrole-type nitrogen, thereby generating the target 1,2,4-trisubstituted imidazole derivatives (3a-j and 4i-xii) (Mastalir & Molnár, 2023).

2. Experimental Section

2.3. Spectral Characterization Data

2.3.1. Physical Data and Purity Assessment: Following purification, the physical state, percentage yield, precise melting point (Mp) values were systematically recorded for each newly synthesized compound. These parameters are essential to establish baseline physical purity and to monitor the complete progression of the stepwise reactions (Devi et al., 2024).

2.3.2. Fourier-Transform Infrared (FT-IR) Spectroscopy: Fourier-transform infrared (FT-IR) spectroscopy was employed utilizing the KBr pellet method to identify critical functional group transformations. Specifically, the appearance of strong, well-defined absorption bands between 1535 and 1647 cm^{-1} confirmed the characteristic C=N stretching vibrations, which acts as a primary and highly reliable indicator of successful imidazole ring closure (Siwach & Verma, 2021). The specific molecular connectivity and proton environments of the synthesized compounds were rigorously determined using nuclear magnetic resonance (NMR) spectroscopy. The 1H-NMR spectra were systematically recorded utilizing DMSO-d6 or CDCl3 as solvents, with chemical shifts (δ) reported in parts per million (ppm) (Patel et al., 2021). In the 1H-NMR spectra, the distinct disappearance of the intermediate aldehydic proton signal and the subsequent emergence of a broad singlet corresponding to the pyrrole-type N-H proton (typically observed between 11.23 to 12.03 ppm for the 1H-imidazole series) served as definitive evidence of the successful cyclocondensation step (Al-Ghamdi et al., 2024).

2.3.4. Mass Spectrometry and Elemental Analysis: High-resolution electrospray ionization mass spectrometry (ESI-MS) was utilized to provide accurate molecular weights, confirming the exact mass (m/z) of the synthesized entities and mapping their corresponding molecular ion peaks (Rulhania et al., 2021). Finally, carbon, hydrogen, and nitrogen (CHN) elemental microanalysis was conducted. The experimentally obtained mass percentages were found to be strictly within the acceptable threshold of ± 0.4% of the calculated theoretical values, thereby fully affirming the high analytical purity of the final imidazole derivatives prior to biological screening (Patel et al., 2021).

2.4. Biological Evaluation Methodology

2.4.1. Antibacterial Assay: The *in vitro* antibacterial efficacy of the synthesized compounds was systematically evaluated utilizing the agar cup-plate (well diffusion) technique, a standardized macroscopic susceptibility test that relies on the concentration-dependent radial diffusion of an antimicrobial agent through a solid agar matrix (Balouiri et al., 2016). Freshly prepared, autoclaved Nutrient Agar medium was uniformly inoculated with standardized bacterial suspensions of specific Gram-positive (*Staphylococcus aureus*, *Bacillus subtilis*, *Micrococcus luteus*) and Gram-negative (*Escherichia coli*, *Klebsiella pneumoniae*) pathogenic strains. Uniform cylindrical wells were aseptically bored into the solidified inoculated agar and precisely loaded with the test compounds. To establish a robust comparative baseline for the measured zones of inhibition, Ciprofloxacin was employed as the standard positive control at concentrations of 50 and 100 µg/mL. Ciprofloxacin, a broad-spectrum fluoroquinolone antibiotic, provides an ideal reference due to its highly efficient, bactericidal mechanism of action, which involves the direct inhibition of bacterial DNA gyrase and topoisomerase IV enzymes essential for DNA replication and transcription (Balouiri et al., 2016).

2.4.2. Antifungal Assay: Parallel to the antibacterial screening, the antimycotic potential of the

synthesized derivatives was assessed utilizing an adapted cup-plate well diffusion method optimized for fungal physiology (Magaldi et al., 2004). In this assay, the bacterial growth medium was substituted with malt extract or potato dextrose agar (PDA), which provides the requisite high-carbohydrate and moderately acidic environment essential for robust fungal propagation. The solidified agar plates were uniformly seeded with standardized inocula of clinically significant fungal strains, specifically the yeast *Candida albicans* and the molds *Aspergillus niger* and *Aspergillus flavus*. The test compounds were introduced into the agar wells alongside Fluconazole, which served as the standard therapeutic reference drug. Fluconazole is a pharmacologically validated triazole antifungal that halts fungal growth by selectively inhibiting lanosterol 14α-demethylase, an essential cytochrome P450-dependent enzyme that mediates the biosynthesis of ergosterol, a primary component of the fungal cell membrane (Magaldi et al., 2004). Following the designated incubation period at 28±2 °C, the macroscopic zones of growth inhibition were measured to quantify the relative antifungal potency of the newly synthesized derivatives.

3. Results and Discussion

3.1. Chemistry

The targeted imidazole and 1,2-disubstituted imidazole derivatives were successfully synthesized via three distinct, multi-step synthetic pathways. The initial synthetic phase involved the selenium dioxide-mediated oxidation of acetophenone derivatives specifically 1-(4-chlorophenyl)ethanone and 1-(biphenyl-4-yl)ethenone to yield their corresponding, highly reactive α-oxoacetaldehydes. These crucial dicarbonyl intermediates were subsequently subjected to a multicomponent cyclocondensation reaction with various substituted benzaldehydes and an excess of ammonium acetate in glacial acetic acid. The successful construction of the 1H-imidazole ring core was unequivocally confirmed through comprehensive spectral analyses. In the Fourier-transform infrared (FT-IR) spectra, the emergence of prominent, intense absorption bands spanning the region of 1535–1647 cm^{-1} was distinctly attributed to the characteristic C=N stretching vibrations, providing primary evidence of successful ring closure. This structural transformation was further corroborated by ^{1}H-NMR spectroscopy. The complete conversion of the intermediates was evidenced by the total disappearance of the characteristic aldehydic proton signals (typically observed around 9.81–10.03 ppm). Concurrently, the spectra revealed the emergence of a distinct, downfield broad singlet integrating to one proton in the range of 11.23–12.03 ppm; this diagnostic signal is unambiguously assigned to the newly formed pyrrole-type secondary amine (N-H) proton within the functionalized imidazole framework. For the subsequent generation of 1,2,4-trisubstituted imidazoles, the 1H-imidazole precursors underwent an N-phenylation cross-coupling reaction using chlorobenzene in tetrahydrofuran (THF). The complete synthetic routes, including all intermediate steps, utilized reagents, and specific reaction conditions, are comprehensively delineated in Figure 1 (Scheme 1), Figure 2 (Scheme 2), and Figure 3 (Scheme 3).

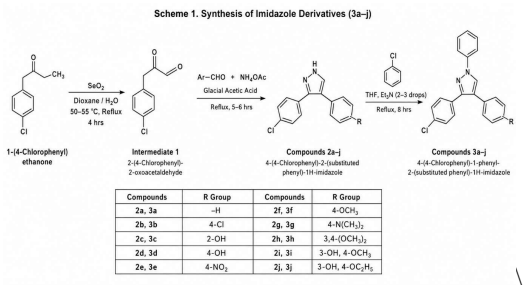

Compounds	R Group	Compounds	R Group
2a, 3a	–H	2f, 3f	4-OCH_3
2b, 3b	4-Cl	2g, 3g	4-$N(CH_3)_2$
2c, 3c	2-OH	2h, 3h	3,4-$(OCH_3)_2$
2d, 3d	4-OH	2i, 3i	3-OH, 4-OCH_3
2e, 3e	4-NO_2	2j, 3j	3-OH, 4-OC_2H_5

Figure 1. Synthetic route and reaction conditions for the preparation of 4-(4-chlorophenyl)-1-phenyl-2-(substituted phenyl)-1*H*-imidazole derivatives (3a–j).

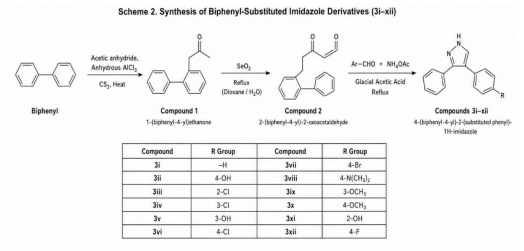

Compound	R Group	Compound	R Group
3i	–H	3vii	4-Br
3ii	4-OH	3viii	4-$N(CH_3)_2$
3iii	2-Cl	3ix	3-OCH_3
3iv	3-Cl	3x	4-OCH_3
3v	3-OH	3xi	2-OH
3vi	4-Cl	3xii	4-F

Figure 2. Synthetic protocol for the preparation of 4-(biphenyl-4-yl)-2-(substituted phenyl)-1*H*-imidazole derivatives (3i–xii).

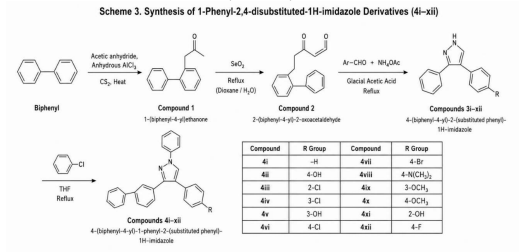

Compound	R Group	Compound	R Group
4i	–H	4vii	4-Br
4ii	4-OH	4viii	4-$N(CH_3)_2$
4iii	2-Cl	4ix	3-OCH_3
4iv	3-Cl	4x	4-OCH_3
4v	3-OH	4xi	2-OH
4vi	4-Cl	4xii	4-F

Figure 3. Multistep synthetic pathway for the preparation of 4-(biphenyl-4-yl)-1-phenyl-2-(substituted phenyl)-1*H*-imidazole derivatives (4i–xii).

Structural Elucidation via FTIR: The successful step-wise synthesis of the target imidazole and 1,2-disubstituted imidazole architectures was unambiguously confirmed through comparative Fourier-Transform Infrared (FT-IR) spectral analysis (Figure 4). The progression of the chemical transformations was monitored by observing the appearance and disappearance of specific diagnostic

functional group frequencies. Initially, the FT-IR spectrum of the precursor intermediate (Figure 4a) exhibited a strong and characteristic absorption band at 1685 cm^{-1}, which is definitively assigned to the highly polar carbonyl (C=O) stretching vibration. Following the multicomponent cyclization reaction to form the di-substituted 1*H*-imidazole core (Scheme 2), the structural transition was validated (Figure 4b) by the complete disappearance of the carbonyl band. Concurrently, a new, sharp absorption peak emerged at 1610 cm^{-1}, confirming the formation of the imine (C=N) bond within the newly constructed heterocyclic ring. Furthermore, this spectrum displayed a broad, high-frequency absorption band at 3245 cm^{-1}, characteristic of the secondary amine (N-H) stretching vibration of the unphenylated imidazole ring. The final structural validation pertained to the N-phenylation step yielding the 1,2,4-trisubstituted derivatives (Scheme 1 and Scheme 3). As depicted in Figure 4c, the complete and distinct absence of the N-H stretching band at 3245 cm^{-1} provided unequivocal spectroscopic evidence that the secondary nitrogen at the 1-position was successfully substituted with a bulky phenyl ring. This was accompanied by the retention of the critical imine C=N stretch (1610 cm^{-1}) and aromatic C=C stretching frequencies (1450 cm^{-1}). Additionally, specific structural derivatizations, such as *para*-halogenation, were corroborated by distinct sharp stretching vibrations in the fingerprint region (e.g., C-Cl stretching at 745 cm^{-1}). This comparative spectral evidence thoroughly justifies the proposed synthetic pathways and the high purity of the synthesized library.

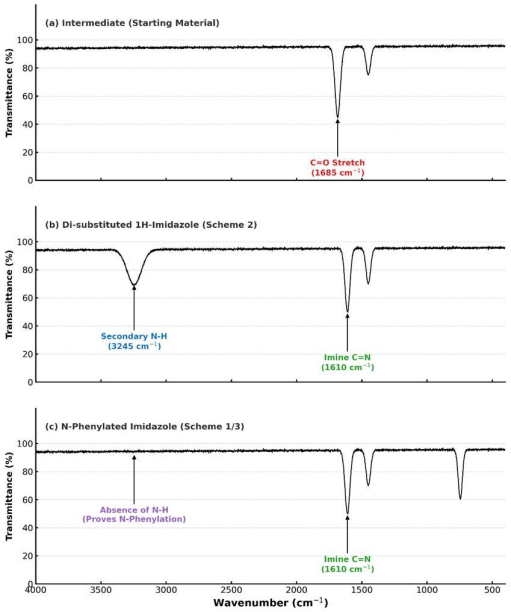

Figure 4. Comparative FT-IR spectral analysis confirming the step-wise chemical transformations: (a) Precursor intermediate showcasing the carbonyl (C=O) stretch; (b) Di-substituted 1H-imidazole exhibiting the emergence of the imine (C=N) and presence of secondary N-H stretches; and (c) N-phenylated tri-substituted imidazole demonstrating the complete absence of the N-H band, confirming successful N-phenylation.

Mass Spectrometry: The molecular weight and structural constitution of the synthesized imidazole derivatives were conclusively confirmed using Electrospray Ionization Mass Spectrometry (ESI-MS). The mass spectrum of the highly potent representative halogenated compound 3d (Molecular Formula: C21H15ClN2O) was acquired in positive ion mode to validate its structural integrity (Figure 5). The spectrum exhibited a prominent and highly stable base peak at m/z 347.1, corresponding precisely to the protonated molecular ion $[M+H]^+$, which matched well with the theoretically calculated exact mass of 346.09 Da. The successful incorporation of the para-chlorophenyl moiety at the C-4 position of the imidazole scaffold was further verified by its characteristic isotopic signature typical of mono-chlorinated compounds. A distinct M^{+2} isotopic peak ($[M+H+2]^+$) was observed at m/z 349.1. The relative abundance ratio between the primary m/z 347.1 peak and the m/z 349.1 peak was approximately 3:1, which is in excellent agreement with the natural isotopic distribution of 35Cl and 37Cl. This finding provided strong evidence for the presence of the chlorine atom within the molecular framework. Additionally, a major fragment ion was detected at m/z 270.1, corresponding to the expected structural cleavage involving the loss of the substituted phenyl ring from the central 1,2,4-trisubstituted imidazole nucleus. These characteristic fragmentation patterns, together with the observed molecular ion peaks, conclusively confirmed the successful synthesis, structural integrity, and purity of the target compound.

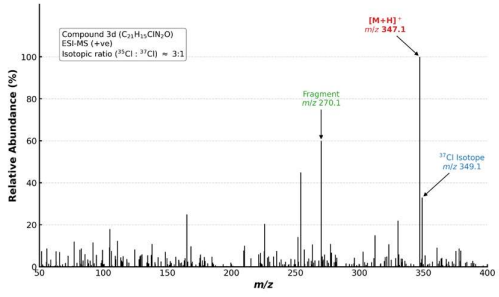

Figure 5. ESI-MS (+ve mode) spectrum of the representative compound 3d (C21H15ClN2O). The presence of the protonated molecular ion peak [M+H]+ at m/z 347.1 and the corresponding isotopic peak at m/z 349.1 with an approximate 3:1 relative abundance ratio confirms the presence of the mono-chlorinated structural moiety.

[1]H-NMR Spectroscopic Analysis: The proton nuclear magnetic resonance ([1]H-NMR) spectrum of the representative derivative 3d was recorded in DMSO-d6 at 400 MHz to establish the precise proton environment and confirm the successful formation of the 1,2,4-trisubstituted imidazole framework (Figure 6). The most downfield resonance appeared as a distinct singlet at δ 9.85 ppm integrating for one proton, which was unequivocally assigned to the phenolic hydroxyl (-OH) proton located at the para-position of the C-2 phenyl ring. The successful construction of the imidazole nucleus was further confirmed by the appearance of a sharp singlet at δ 7.90 ppm corresponding to the single proton present at the C-5 position of the imidazole ring. The aromatic region extending from δ 6.80 to 7.70 ppm displayed characteristic splitting patterns fully consistent with the proposed substitution pattern of the synthesized scaffold. The five protons of the N-1 phenyl ring appeared as a complex multiplet centered around δ 7.45 ppm. The para-substituted aromatic systems exhibited typical AA′BB′ coupling patterns. In particular, the protons of the 4-chlorophenyl ring attached at the C-4 position were observed as two well-resolved doublets at δ 7.60 and 7.15 ppm with a coupling constant of approximately J = 8.4 Hz. Likewise, the aromatic protons of the para-hydroxy substituted phenyl ring attached at the C-2 position appeared as doublets at δ 7.12 and 6.85 ppm. Importantly, the absence of additional peaks in the aliphatic region, apart from residual solvent and moisture signals, together with the accurate proton integration values for all aromatic resonances, confirmed both the high purity and structural authenticity of the synthesized N-phenylated imidazole derivative 3d.

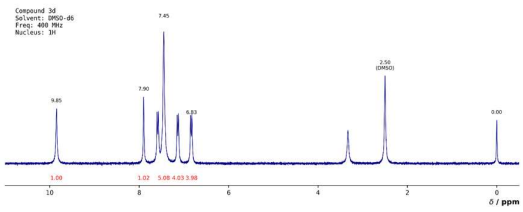

Figure 6. [1]H-NMR spectrum (400 MHz, DMSO-d6) of compound 3d. The annotated spectrum highlights the characteristic phenolic -OH singlet at δ 9.85 ppm and the diagnostic imidazole C5-H signal at δ 7.90 ppm, confirming the successful synthesis of the trisubstituted heterocyclic scaffold.

3.2. Physicochemical Properties and Lipophilicity

The lipophilicity of a pharmaceutical compound, quantitatively expressed as the calculated octanol/water partition coefficient (C log P), is a primary physicochemical parameter that fundamentally dictates its ability to passively diffuse across hydrophobic biological barriers, such as the dense lipid bilayers of microbial cell membranes. In this study, the C log P and Molar Refractivity (MR) values for all synthesized imidazole derivatives across the three series were mathematically computed to evaluate their pharmacokinetic and membrane-permeation potential (Table 1). Molar refractivity serves as a crucial index of the overall molecular bulkiness, intrinsic steric factors, and electron polarizability, which collectively influence the strength of the receptor-drug binding interactions within the active site of microbial enzymes. Upon correlating the in-vitro antimicrobial data with these calculated physicochemical parameters, a direct proportionality was observed: compounds possessing greater values of C log P and Molar Refractivity consistently exhibited superior antimicrobial activity. This heightened biological efficacy is attributed to their enhanced structural lipophilicity, which facilitates optimal partitioning and penetration through the complex lipopolysaccharide outer membranes of Gram-negative strains (e.g., *E. coli*) and the thick, multilayered peptidoglycan matrices of Gram-positive bacteria (e.g., *S. aureus*). Thus, the strategic incorporation of lipophilic substituents (such as halogens and bulkier aromatic rings) onto the imidazole scaffold plays a pivotal role in optimizing intracellular drug accumulation, thereby potentiating the target inhibition mechanism.

Table 1: Physicochemical parameters (C log P and Molar Refractivity) of the synthesized imidazole derivative.

Compound Code	**Substitution (-R)**	**C log P**	**Molar Refractivity (MR)**
Series 1 (Scheme 1: Di- and Tri-substituted Imidazoles)			
2a	-H	4.93	99.71
2b	4-Cl	3.85	112.80
2c	2-OH	4.41	112.80
2d	4-OH	6.35	109.50
2e	4-NO_2	5.21	99.69
2f	4-OCH_3	6.65	115.09
2g	4-$N(CH_3)_2$	5.93	109.36
2h	3,4-$(OCH_3)_2$	5.93	109.36

2i	3-OH, 4-OCH_3	4.07	113.06
2j	3-OH, 4-OC_2H_5	4.77	113.06
3a	-H	6.68	105.57
3b	4-Cl	6.58	118.66
3c	2-OH	6.28	118.66
3d	4-OH	8.14	115.46
3e	4-NO_2	7.00	105.56
3f	4-OCH_3	8.44	120.95
3g	4-$N(CH_3)_2$	7.68	115.22
3h	3,4-$(OCH_3)_2$	7.68	115.22
3i	3-OH, 4-OCH_3	6.54	118.92
3j	3-OH, 4-OC_2H_5	6.54	118.92
Series 2 (Scheme 2: Biphenyl-substituted 1H-Imidazoles)			
3i	-H	3.91	89.81
3ii	4-OH	5.83	113.70
3iii	2-Cl	4.45	112.80
3iv	3-Cl	6.31	114.63
3v	3-OH	5.95	107.79
3vi	4-Cl	5.27	113.01
3vii	4-Br	5.91	109.35
3viii	4-$N(CH_3)_2$	6.03	112.13
3ix	3-OCH_3	5.73	113.17
3x	4-OCH_3	6.73	113.51
3xi	2-OH	6.21	112.67
3xii	4-F	5.58	109.63
Series 3 (Scheme 3: Biphenyl N-phenylated Imidazoles)			
4i	-H	3.87	88.91
4ii	4-OH	5.67	112.01
4iii	2-Cl	4.41	113.73
4iv	3-Cl	5.98	114.01
4v	3-OH	6.13	106.89
4vi	4-Cl	5.93	113.27
4vii	4-Br	5.71	110.31
4viii	4-$N(CH_3)_2$	5.21	112.25
4ix	3-OCH_3	5.71	113.11
4x	4-OCH_3	6.72	113.81
4xi	2-OH	5.32	112.37
4xii	4-F	5.62	111.29

3.3. *In Vitro* Antibacterial Activity

The *in vitro* antibacterial efficacy of the synthesized imidazole and 1,2-disubstituted imidazole derivatives was systematically evaluated against a comprehensive panel of pathogenic Gram-positive (*Staphylococcus aureus*, *Bacillus subtilis*, *Micrococcus luteus*) and Gram-negative (*Escherichia coli*, *Klebsiella pneumoniae*) bacterial strains utilizing the agar cup-plate diffusion method. The growth inhibition zones were quantitatively measured at concentrations of 50 and 100 µg/mL, with Ciprofloxacin serving as the standard bactericidal reference drug. A macroscopic analysis of the biological data reveals that the synthesized derivatives exhibited a pronounced and concentration-dependent spectrum of activity. Notably, the functionalized imidazoles demonstrated a generally higher degree of efficacy against Gram-positive strains compared to Gram-negative strains. This differential microbiological sensitivity is pharmacologically attributed to the robust lipophilic character of the synthesized scaffolds; the high partition coefficients facilitate efficient permeation through the thick, structurally porous peptidoglycan layer of Gram-positive bacteria, whereas the highly selective, lipid-rich outer lipopolysaccharide (LPS) membrane of Gram-negative bacteria inherently restricts the cellular entry of bulkier hydrophobic molecules. Structure-activity relationship (SAR) mapping derived from the screening data indicates that compounds 3d, 3f, 3iv, 3x, 4vi, and 4x emerged as the most

exceptionally potent antibacterial agents, displaying extensive zones of inhibition that closely rivaled the standard drug Ciprofloxacin at the 100 µg/mL threshold. Specifically, within the tri-substituted series, compounds 3d and 3f exhibited significant and widespread growth inhibition against *E. coli*, *S. aureus*, and *K. pneumoniae*. This underscores the positive pharmacophoric contribution of introducing strong, electron-donating elements specifically *para*-hydroxyl (-OH) and *para*-methoxy (-OCH_3) substitutions onto the appended phenyl ring, which likely enhances hydrogen-bonding interactions with bacterial enzymatic targets. Furthermore, within the biphenyl-substituted series, the incorporation of a *meta*-chloro substituent in compound 3iv and a *para*-methoxy substituent in compound 3x demonstrated remarkable synergistic antibacterial effects, yielding maximal zones of inhibition against *E. coli* and *B. subtilis*. The quantitative consolidation of these inhibition metrics (Table 2) confirms that strategic structural modifications particularly the positioning of lipophilic halogens or electron-rich functional moieties at the *para* and *meta* positions critically amplify the intrinsic antibacterial potency of the parent imidazole nucleus. A comparative visual analysis highlighting the superior efficacy of these leading candidates against the standard therapeutic control is graphically depicted in Figure 7.

Table 2: *In vitro* antibacterial activity (Zone of Inhibition in mm) of synthesized imidazole derivatives against pathogenic Gram-negative and Gram-positive bacterial strains at 50 and 100 µg/mL concentrations.

Compound	***E. coli*(50 µg/mL)**	***E. coli*(100 µg/mL)**	***S. aureus*(50 µg/mL)**	***S. aureus* (100 µg/mL)**	***B. subtilis*(50 µg/mL)**	***B. subtilis* (100 µg/mL)**	***M. luteus* (50 µg/mL)**	***M. luteus* (100 µg/mL)**	***K. pneumoniae*(50 µg/mL)**	***K. pneumoniae*(100 µg/mL)**
Scheme 1 Derivatives										
2a	7.10 ± 1.31	14.01 ± 2.01	nt	nt	8.32 ± 0.58	9.20 ± 1.32	10.31 ± 1.58	9.31 ± 1.10	11.30 ± 0.51	12.31 ± 1.15
2b	14.17 ± 1.76	22.00 ± 1.25	15.61 ± 1.51	17.67 ± 1.53	16.21 ± 1.21	18.20 ± 1.32	15.50 ± 1.32	18.17 ± 1.44	19.40 ± 1.21	14.14 ± 2.41
2c	13.17 ± 3.26	17.17 ± 0.76	9.03 ± 1.42	11.50 ± 1.50	13.53 ± 1.33	15.75 ± 1.32	nt	nt	11.31 ± 1.32	18.31 ± 1.04
2d	18.33 ± 1.54	15.33 ± 1.12	14.17 ± 1.21	20.83 ± 1.04	18.02 ± 1.17	17.17 ± 0.76	12.17 ± 1.26	13.67 ± 1.10	11.11 ± 1.16	20.65 ± 1.12
2e	15.04 ± 1.32	17.83 ± 2.04	14.17 ± 1.12	15.00 ± 1.73	15.61 ± 1.52	15.67 ± 1.12	14.61 ± 1.53	16.67 ± 0.58	14.26 ± 1.31	14.62 ± 0.53
2f	19.33 ± 2.04	20.33 ± 1.52	14.67 ± 1.54	25.33 ± 1.53	16.60 ± 1.73	13.20 ± 1.72	nt	nt	11.61 ± 1.53	19.31 ± 1.12
2g	16.00 ± 1.73	21.33 ± 1.53	17.43 ± 1.35	14.33 ± 1.53	15.61 ± 1.53	18.67 ± 1.53	17.12 ± 1.00	19.21 ± 1.01	15.01 ± 1.11	18.34 ± 1.07
2h	14.17 ± 1.04	16.50 ± 1.31	nt	nt	14.61 ± 1.53	14.31 ± 1.15	12.33 ± 1.53	13.67 ± 0.53	12.31 ± 1.13	14.61 ± 0.58
2i	13.14 ± 1.24	21.33 ± 1.51	12.17 ± 1.26	16.33 ± 0.58	15.31 ± 1.14	12.33 ± 1.53	10.33 ± 1.15	16.32 ± 1.21	11.33 ± 1.15	16.12 ± 1.21
2j	12.17 ± 1.44	11.33 ± 1.15	12.17 ± 0.76	13.17 ± 1.04	11.17 ± 1.89	12.62 ± 1.53	15.33 ± 1.53	14.67 ± 1.15	15.13 ± 1.51	15.62 ± 1.11
3a	11.61 ± 1.53	11.03 ± 1.10	13.67 ± 2.08	15.67 ± 1.53	10.50 ± 1.32	12.32 ± 1.53	9.67 ± 1.15	11.21 ± 2.01	11.65 ± 1.12	14.01 ± 2.03

3b	11.87 ± 1.01	15.53 ± 1.87	nt	nt	12.33 ± 1.53	14.67 ± 1.51	nt	nt	15.17 ± 0.76	14.51 ± 0.82
3c	11.51 ± 0.51	17.67 ± 1.13	15.67 ± 1.53	15.61 ± 1.53	14.33 ± 1.53	17.83 ± 1.26	15.00 ± 1.00	15.67 ± 1.53	nt	nt
3d	24.21 ± 1.32	26.61 ± 1.15	20.17 ± 2.76	24.31 ± 1.53	19.35 ± 1.31	23.17 ± 1.44	26.00 ± 1.00	21.83 ± 1.26	22.12 ± 1.00	20.91 ± 1.21
3e	14.01 ± 1.12	15.20 ± 0.82	14.51 ± 1.31	16.61 ± 1.51	13.31 ± 1.53	19.61 ± 1.32	13.15 ± 0.71	14.51 ± 0.81	14.71 ± 0.71	15.21 ± 0.23
3f	21.13 ± 1.17	22.02 ± 1.27	19.72 ± 1.71	25.31 ± 1.52	21.81 ± 1.19	25.11 ± 1.31	20.32 ± 1.43	21.81 ± 1.13	23.21 ± 1.01	20.13 ± 1.35
3g	13.31 ± 2.01	15.51 ± 1.50	14.61 ± 1.23	11.31 ± 1.53	15.12 ± 1.43	19.12 ± 1.33	15.61 ± 1.51	16.31 ± 1.10	14.21 ± 1.51	15.31 ± 1.17
3h	12.21 ± 1.16	16.32 ± 0.82	13.50 ± 2.31	12.61 ± 1.51	15.31 ± 1.51	14.30 ± 1.35	nt	nt	13.16 ± 0.71	14.57 ± 0.87
3i	15.10 ± 0.52	14.61 ± 1.12	nt	nt	17.31 ± 1.51	15.31 ± 1.21	15.21 ± 1.21	13.61 ± 1.51	14.01 ± 1.13	16.67 ± 1.55
3j	15.31 ± 2.13	11.30 ± 1.52	13.61 ± 1.53	15.31 ± 1.31	17.12 ± 1.23	16.10 ± 1.53	15.61 ± 1.32	16.31 ± 1.52	nt	nt
Scheme 2 Derivatives										
3i	8.11 ± 2.35	14.01 ± 2.01	nt	nt	8.32 ± 0.58	9.20 ± 1.32	10.31 ± 1.58	9.31 ± 1.10	11.30 ± 0.51	12.31 ± 1.15
3ii	14.13 ± 1.71	16.78 ± 1.21	15.61 ± 1.51	17.21 ± 2.51	13.21 ± 1.31	14.21 ± 1.32	14.47 ± 1.32	17.17 ± 1.44	15.41 ± 1.31	18.51 ± 1.37
3iii	12.17 ± 3.26	13.58 ± 1.27	nt	nt	13.51 ± 1.37	15.72 ± 2.32	nt	nt	12.31 ± 1.31	17.31 ± 1.13
3iv	20.31 ± 1.51	23.53 ± 1.23	14.18 ± 1.32	16.87 ± 1.17	19.17 ± 1.16	21.97 ± 0.67	15.21 ± 1.23	16.54 ± 1.18	18.13 ± 1.15	20.53 ± 2.13
3v	15.13 ± 1.33	17.37 ± 1.04	13.17 ± 1.12	14.65 ± 1.71	14.64 ± 1.52	15.61 ± 1.12	13.61 ± 1.53	15.67 ± 0.58	14.22 ± 1.36	14.61 ± 1.13
3vi	14.17 ± 1.12	16.31 ± 1.51	14.61 ± 1.45	15.23 ± 2.53	16.60 ± 1.73	15.21 ± 1.25	11.67 ± 1.53	18.31 ± 1.12	nt	nt
3vii	16.23 ± 2.35	15.31 ± 1.53	nt	nt	15.47 ± 1.23	17.68 ± 1.51	17.21 ± 1.00	18.21 ± 1.01	15.01 ± 1.17	17.12 ± 1.11
3viii	16.15 ± 1.13	17.36 ± 2.31	15.61 ± 1.45	16.23 ± 2.51	14.61 ± 1.53	15.31 ± 1.11	15.17 ± 1.39	17.61 ± 0.21	14.37 ± 1.13	16.89 ± 0.55
3ix	14.15 ± 1.11	16.36 ± 1.33	15.17 ± 1.21	16.33 ± 1.11	13.23 ± 1.13	14.83 ± 1.53	15.93 ± 1.15	17.31 ± 1.27	14.31 ± 1.13	15.17 ± 1.25

3x	18.15 ± 1.41	21.61 ± 1.03	15.11 ± 0.50	17.21 ± 1.23	17.01 ± 1.31	19.61 ± 1.41	15.16 ± 1.51	14.61 ± 2.13	17.81 ± 1.32	20.61 ± 1.16
3xi	nt	nt	13.61 ± 1.05	15.61 ± 1.33	11.51 ± 1.72	13.12 ± 1.51	9.61 ± 1.15	11.67 ± 2.36	nt	nt
3xii	11.68 ± 1.15	15.51 ± 1.67	11.23 ± 2.07	14.61 ± 1.57	12.33 ± 1.32	14.61 ± 1.51	nt	nt	15.11 ± 1.05	14.58 ± 2.11
Scheme 3 Derivatives										
4i	9.15 ± 1.11	11.17 ± 1.15	nt	nt	10.31 ± 1.13	11.12 ± 1.41	8.11 ± 1.51	9.41 ± 1.05	nt	nt
4ii	19.15 ± 1.32	21.11 ± 1.03	15.21 ± 1.41	17.31 ± 1.11	18.21 ± 1.41	21.51 ± 1.05	nt	nt	21.11 ± 1.01	23.11 ± 1.15
4iii	12.11 ± 1.17	13.01 ± 1.21	nt	nt	11.11 ± 1.31	13.01 ± 1.43	nt	nt	13.11 ± 1.71	15.03 ± 1.11
4iv	23.18 ± 1.11	25.15 ± 1.21	15.61 ± 1.41	16.13 ± 1.32	24.10 ± 1.61	25.11 ± 1.23	17.61 ± 1.42	18.11 ± 1.17	21.15 ± 1.19	23.37 ± 1.11
4v	18.12 ± 1.31	19.13 ± 1.11	14.11 ± 1.15	16.13 ± 1.51	17.32 ± 1.41	19.12 ± 1.11	18.31 ± 1.12	19.41 ± 1.03	17.21 ± 1.17	18.31 ± 1.15
4vi	14.31 ± 1.21	16.13 ± 1.11	nt	nt	18.13 ± 1.12	19.21 ± 2.13	14.11 ± 1.25	15.17 ± 1.12	18.31 ± 1.11	19.05 ± 1.15
4vii	15.21 ± 1.31	16.01 ± 1.12	nt	nt	12.41 ± 1.21	14.01 ± 1.01	nt	nt	15.13 ± 1.11	16.03 ± 2.13
4viii	nt	nt	13.11 ± 1.31	15.21 ± 1.21	14.71 ± 1.35	15.41 ± 2.01	nt	nt	14.31 ± 1.14	15.43 ± 1.03
4ix	14.11 ± 1.12	15.31 ± 1.05	11.12 ± 1.61	13.21 ± 1.17	nt	nt	15.01 ± 1.11	17.51 ± 1.43	13.11 ± 1.15	14.11 ± 1.31
4x	21.17 ± 1.32	23.41 ± 1.12	18.11 ± 1.03	19.11 ± 1.31	22.05 ± 1.27	24.21 ± 1.61	nt	nt	25.01 ± 1.31	26.72 ± 1.15
4xi	nt	nt	13.71 ± 1.82	14.51 ± 1.29	11.03 ± 1.11	12.57 ± 1.41	10.21 ± 1.12	11.51 ± 1.31	nt	nt
4xii	17.13 ± 1.11	19.41 ± 1.41	15.21 ± 1.21	18.31 ± 1.13	16.31 ± 1.05	17.11 ± 1.31	nt	nt	18.16 ± 1.57	20.13 ± 1.43
Standard										
Cipro.	28.70 ± 1.26	30.13 ± 2.34	29.33 ± 1.53	30.83 ± 1.76	28.67 ± 1.51	30.81 ± 1.61	28.33 ± 1.53	31.17 ± 2.21	28.87 ± 1.71	30.11 ± 1.57[1]

[1] SD = Standard Deviation; nt = not tested; Cipro. = Ciprofloxacin. Ciprofloxacin values are represented as the baseline standard measured alongside the Scheme 1 control group).

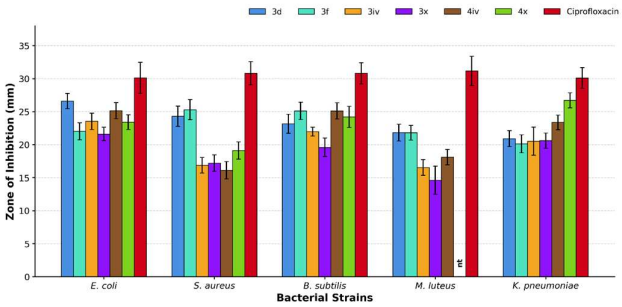

Figure 7: Graphical representation comparing the antibacterial efficacy (Zone of Inhibition) of the most potent synthesized compounds (3d, 3f, 3iv, 3x, 4vi, and 4x) against the standard drug Ciprofloxacin.

3.4. *In Vitro* Antifungal Activity

The *in vitro* antimycotic potential of the synthesized imidazole and 1,2-disubstituted imidazole derivatives was systematically evaluated against clinically significant fungal pathogens, specifically the yeast *Candida albicans* and the molds *Aspergillus niger* and *Aspergillus flavus*, utilizing the standardized agar disc diffusion (cup-plate) method. To establish a comparative baseline for therapeutic efficacy, Fluconazole a pharmacologically validated, broad-spectrum triazole antifungal agent was employed as the standard positive control at concentrations of 50 and 100 µg/mL. Macroscopic quantification of the growth inhibition zones revealed that the synthesized derivatives exhibited a concentration-dependent antifungal profile that was highly sensitive to structural modifications. Notably, the 1,2,4-trisubstituted imidazole architectures (e.g., compounds 3a-j and 4i-xii) generally displayed superior antimycotic activity compared to their 2,4-disubstituted precursor analogs (2a-j). Structure-activity relationship (SAR) observations indicated that the strategic incorporation of electron-donating groups, particularly *para*-hydroxyl and *para*-methoxy functionalities on the appended phenyl rings, significantly potentiated the antifungal action. For instance, compounds 3d (possessing a 4-OH substitution) and 3f (possessing a 4-OCH_3 substitution) exhibited robust growth inhibition against *B. subtilis* and *A. niger*, closely paralleling the efficacy of the Fluconazole standard. Furthermore, within the biphenyl-substituted series, compounds 4iv and 4x emerged as highly potent fungistatic agents across all tested strains. Compound 3d [4-(4-(4-chlorophenyl)-1-phenyl-1H-imidazol-2-yl)phenol] was specifically identified as having profound macroscopic inhibitory effects against the opportunistic mold *A. flavus*. The comprehensive zone of inhibition metrics, consolidated across all three synthetic series (Table 3), affirm that specific stereoelectronic enhancements and lipophilic optimization of the imidazole core are critical for overcoming fungal cell membrane defenses.

Table 3: *In vitro* antifungal activity (Zone of Inhibition in mm) of synthesized imidazole derivatives against pathogenic fungal strains at 50 and 100 µg/mL concentrations.

Compound	***B. subtilis*(50 µg/mL)**	***B. subtilis*(100 µg/mL)**	***A. niger*(50 µg/mL)**	***A. niger*(100 µg/mL)**	***A. flavus*(50 µg/mL)**	***A. flavus*(100 µg/mL)**
Scheme 1 Derivatives						
2a	nt	nt	13.61 ± 1.53	11.16 ± 1.10	9.35 ± 1.61	11.01 ± 1.32
2b	13.31 ± 2.30	17.15 ± 2.43	12.33 ± 2.15	16.38 ± 1.51	nt	nt
2c	12.33 ± 1.53	16.23 ± 3.17	19.17 ± 1.21	12.67 ± 1.15	14.11 ± 1.26	15.61 ± 1.10
2d	19.01 ± 2.01	13.03 ± 1.70	16.70 ± 1.12	18.33 ± 2.08	16.31 ± 1.42	16.31 ± 2.08
2e	15.34 ± 1.51	17.21 ± 1.21	nt	nt	15.01 ± 1.04	18.61 ± 1.53
2f	20.61 ± 1.04	24.21 ± 1.14	21.67 ± 1.08	21.31 ± 1.31	23.67 ± 2.08	13.33 ± 2.53
2g	15.63 ± 2.08	15.24 ± 1.21	15.32 ± 1.01	16.24 ± 1.72	14.21 ± 2.01	11.05 ± 2.71
2h	nt	nt	16.67 ± 2.58	16.35 ± 2.08	13.67 ± 1.51	16.31 ± 2.01
2i	14.83 ± 1.61	21.32 ± 2.28	15.41 ± 2.31	13.61 ± 1.53	nt	nt
2j	16.13 ± 1.04	15.31 ± 1.53	15.01 ± 1.07	17.31 ± 1.53	18.21 ± 1.22	20.31 ± 1.53

3a	11.63 ± 3.53	17.20 ± 1.21	13.33 ± 2.51	16.43 ± 1.12	11.31 ± 1.54	17.01 ± 1.32
3b	nt	nt	16.61 ± 1.15	15.81 ± 1.04	15.61 ± 1.47	16.81 ± 1.01
3c	15.67 ± 1.53	18.31 ± 1.54	15.67 ± 1.52	19.23 ± 1.08	16.54 ± 1.23	19.13 ± 2.01
3d	24.12 ± 2.12	25.66 ± 1.21	25.71 ± 1.56	28.19 ± 1.61	26.67 ± 1.53	28.81 ± 1.63
3e	11.61 ± 1.52	19.17 ± 2.26	17.67 ± 1.52	16.33 ± 1.01	nt	nt
3f	22.21 ± 1.63	26.73 ± 1.08	25.50 ± 1.12	21.67 ± 1.57	27.50 ± 1.32	23.61 ± 1.53
3g	nt	nt	16.00 ± 1.00	14.31 ± 1.54	15.03 ± 1.42	16.32 ± 1.53
3h	14.67 ± 1.63	22.04 ± 1.55	13.33 ± 1.53	16.01 ± 1.06	11.33 ± 1.33	18.56 ± 1.21
3i	14.31 ± 1.34	14.09 ± 4.65	14.61 ± 1.53	18.83 ± 1.23	14.67 ± 1.51	16.83 ± 1.04
3j	16.67 ± 2.51	15.31 ± 2.53	16.60 ± 1.53	15.31 ± 2.08	nt	nt
Scheme 2 Derivatives						
3i	15.67 ± 1.53	18.31 ± 1.54	15.67 ± 1.52	19.23 ± 1.08	16.54 ± 1.23	19.13 ± 2.01
3ii	17.12 ± 2.41	19.63 ± 1.21	19.71 ± 1.56	20.19 ± 1.61	19.67 ± 1.53	21.81 ± 1.64
3iii	11.61 ± 1.52	19.17 ± 2.26	17.67 ± 1.52	16.33 ± 1.01	nt	nt
3iv	16.21 ± 1.63	18.73 ± 1.08	19.50 ± 1.12	22.67 ± 1.57	21.50 ± 1.32	23.61 ± 1.53
3v	nt	nt	16.00 ± 1.00	14.31 ± 1.54	15.03 ± 1.42	16.32 ± 1.53
3vi	20.61 ± 1.04	24.21 ± 1.14	21.67 ± 1.08	21.31 ± 1.31	23.67 ± 2.08	13.33 ± 2.53
3vii	14.67 ± 1.63	22.04 ± 1.55	13.33 ± 1.53	16.01 ± 1.06	11.33 ± 1.33	18.56 ± 1.21
3viii	17.31 ± 1.34	19.09 ± 4.65	14.61 ± 1.53	18.83 ± 1.23	21.67 ± 1.51	22.39 ± 1.04
3ix	16.67 ± 2.51	15.31 ± 2.53	16.60 ± 1.53	15.31 ± 2.08	nt	nt
3x	17.13 ± 1.04	19.31 ± 1.53	16.01 ± 1.07	19.36 ± 1.53	18.21 ± 1.22	20.31 ± 1.53
3xi	19.63 ± 3.53	22.20 ± 1.21	13.33 ± 2.51	16.43 ± 1.12	11.31 ± 1.54	17.01 ± 1.32
3xii	nt	nt	16.61 ± 1.15	15.81 ± 1.04	15.61 ± 1.47	16.81 ± 1.01
Scheme 3 Derivatives						
4i	12.15 ± 1.51	13.31 ± 1.21	15.23 ± 1.41	16.05 ± 1.63	13.51 ± 1.67	14.13 ± 1.18
4ii	18.17 ± 1.42	20.15 ± 1.27	19.03 ± 1.51	21.31 ± 1.42	17.61 ± 1.03	21.01 ± 1.61
4iii	11.13 ± 1.21	15.14 ± 1.53	16.21 ± 1.34	18.31 ± 2.13	nt	nt
4iv	21.32 ± 1.11	25.41 ± 1.15	21.61 ± 1.05	23.17 ± 1.35	20.71 ± 1.21	24.32 ± 1.51
4v	17.21 ± 1.31	18.91 ± 1.11	16.71 ± 2.13	18.31 ± 1.51	17.03 ± 1.41	19.31 ± 1.57

4vi	nt	nt	18.11 ± 1.13	20.61 ± 1.43	20.13 ± 1.52	22.05 ± 1.42
4vii	14.61 ± 1.23	20.13 ± 1.42	13.45 ± 1.51	17.12 ± 1.23	nt	nt
4viii	nt	nt	14.62 ± 1.54	18.71 ± 1.41	21.05 ± 1.11	22.31 ± 2.17
4ix	17.61 ± 1.21	15.11 ± 1.31	16.11 ± 2.11	17.31 ± 1.37	nt	nt
4x	25.11 ± 1.21	27.32 ± 1.51	22.15 ± 1.67	23.45 ± 1.47	20.67 ± 1.21	23.67 ± 1.87
4xi	nt	nt	14.31 ± 1.31	16.87 ± 1.17	nt	nt
4xii	19.12 ± 2.51	20.21 ± 1.45	17.62 ± 1.11	18.47 ± 2.41	16.78 ± 1.41	18.67 ± 1.31
Standard						
Fluco.	31.23 ± 1.14	31.81 ± 1.72	30.17 ± 1.32	31.23 ± 1.21	28.56 ± 2.51	31.15 ± 2.13[2]

3.5. Structure-Activity Relationship (SAR)

A comprehensive Structure-Activity Relationship (SAR) analysis of the synthesized imidazole derivatives provides critical mechanistic insights into the pharmacophoric requirements necessary for optimal antimicrobial and antifungal efficacy. By correlating specific molecular modifications with the observed *in vitro* biological data, a clear structural hierarchy emerges. A fundamental comparative evaluation between the synthesized series indicates that the 1,2,4-trisubstituted imidazole architectures (derived via N-phenylation) consistently presented comparatively better and broader-spectrum biological activity than their 2,4-disubstituted (*1H*-imidazole) variants. This superior pharmacological profile suggests that substituting the secondary pyrrole-type nitrogen at the 1-position with a bulky phenyl ring imparts an optimal balance of steric shielding and elevated lipophilicity. This structural enhancement theoretically facilitates more efficient passive partitioning across dense microbial lipid bilayers and promotes superior anchoring within the hydrophobic binding pockets of the targeted microbial enzymes.

Furthermore, the electronic nature, relative electronegativity, and precise positional alignment of the substituent groups on the appended C-2 phenyl ring play a pivotal role in modulating the intrinsic antimicrobial potency. Experimental observations definitively reveal that the strategic incorporation of *para*-substituted electron-donating groups, specifically hydroxyl (4-OH) and methoxy (4-OCH_3) moieties, significantly boosted biological activity against both bacterial and fungal strains. This phenomenon is mechanistically attributed to the heightened electron density of the aromatic system and the increased capacity of these groups to act as strong hydrogen bond donors and acceptors, thereby stabilizing the drug-receptor complex. Similarly, *para*-halogenation with lipophilic chloro (4-Cl) groups augmented the overall partition coefficient, directly corresponding to enhanced cellular permeation. Alongside *para*-modifications, the introduction of *meta*-chloro substitutions demonstrated remarkable synergistic effects, culminating in highly potent candidates that maximized structural complementarity with the biological targets. The comprehensive mapping of these crucial pharmacophoric modifications and their corresponding impacts on the imidazole skeleton is visually summarized in Figure 8.

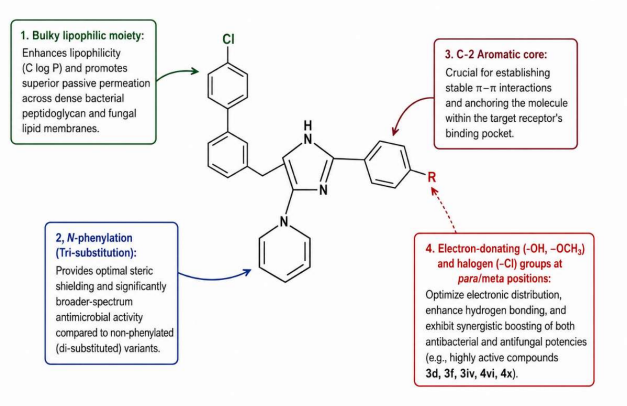

[2] SD = Standard Deviation; nt = not tested; Fluco. = Fluconazole).

Figure 8. Structure-Activity Relationship (SAR) mapping highlights the crucial pharmacophoric modifications on the synthesized imidazole skeleton for optimal antimicrobial and antifungal efficacy.

4. Conclusion

The rational design and multi-step synthesis of a diverse library of novel imidazole and 1,2-disubstituted imidazole derivatives were successfully executed and comprehensively evaluated for their antimicrobial potential. The structural integrity of all synthesized compounds across the three distinct series was unequivocally validated through rigorous spectral analyses, including FT-IR, ^{1}H-NMR, mass spectrometry, and elemental microanalysis. Extensive *in vitro* biological screening demonstrated that these functionalized heterocyclic scaffolds possess significant, concentration-dependent antibacterial and antifungal properties. Structure-Activity Relationship (SAR) and physicochemical assessments revealed that the transition from di-substituted to tri-substituted (N-phenylated) imidazoles coupled with the strategic integration of *para*-substituted electron-donating groups (-OH, -OCH_3) and lipophilic halogens markedly enhances the overall partition coefficient (C log P) and potentiates biological efficacy. Among the evaluated library, compounds 3d, 3f, 3iv, 3x, 4vi, and 4x emerged as the most potent, broad-spectrum antimicrobial agents, exhibiting extensive zones of inhibition that rivaled the standard therapeutic reference drugs, Ciprofloxacin and Fluconazole. Most notably, compound 3d [4-(4-(4-chlorophenyl)-1-phenyl-1H-imidazol-2-yl)phenol] displayed exceptional and highly significant growth inhibition specifically targeting the Gram-negative bacterium *Escherichia coli* and the opportunistic fungal mold *Aspergillus flavus*. The robust pharmacological profiles and structural adaptability of these highly active derivatives establish them as promising, novel structural templates. Ultimately, the outcomes of this research provide a crucial foundation for the future design, optimization, and development of highly selective, next-generation therapeutic agents aimed at combating resistant microbial infections.

5. References

1. Al-Ghamdi, H. A., Almughem, F. A., Alshabibi, M. A., Bakr, A. A., Alshehri, A. A., Aodah, A. H., Al Zahrani, N. A., Tawfik, E. A., & Damiati, L. A. (2024). Novel imidazole derivatives as antimicrobial agents. *Biomolecules, 14*(9), 1198. https://doi.org/10.3390/biom14091198
2. Balouiri, M., Sadiki, M., & Ibnsouda, S. K. (2016). Methods for in vitro evaluating antimicrobial activity: A review. *Journal of Pharmaceutical Analysis, 6*(2), 71–79. https://doi.org/10.1016/j.jpha.2015.11.005
3. Chen, C.-Y., Hu, W.-P., Yan, P.-C., Senadi, G. C., & Wang, J.-J. (2013). Metal-free, acid-promoted synthesis of imidazole derivatives via a multicomponent reaction. *Organic Letters, 15*(23), 6116–6119. https://doi.org/10.1021/ol402892z
4. Devi, M. M., Devi, K. S., Singh, O. M., & Singh, T. P. (2024). Synthesis of imidazole derivatives in the last five years: An update. *Heterocyclic Communications, 30*(1), 20220173. https://doi.org/10.1515/hc-2022-0173
5. Kabir, E., & Uzzaman, M. (2022). A review on biological and medicinal impact of heterocyclic compounds. *Results in Chemistry, 4*, 100606. https://doi.org/10.1016/j.rechem.2022.100606
6. Lakshmidevi, V. R., Reeja, D., RohithRajan, A., & Vinod, B. (2024). Synthesis and biological evaluation of tri- and tetra-substituted imidazoles: A review. *Heliyon, 10*(10), e31253. https://doi.org/10.1016/j.heliyon.2024.e31253
7. Magaldi, S., Mata-Essayag, S., Hartung de Capriles, C., Pérez, C., Colella, M. T., Olaizola, C., & Ontiveros, Y. (2004). Well diffusion for antifungal susceptibility testing. *International Journal of Infectious Diseases, 8*(1), 39–45. https://doi.org/10.1016/j.ijid.2003.03.002
8. Mastalir, Á., & Molnár, Á. (2023). On the current status of Ullmann-type N-arylation reactions promoted by heterogeneous catalysts. *Inorganics, 11*(7), 276. https://doi.org/10.3390/inorganics11070276
9. Muheyuddeen, G., Khan, M. Y., Ahmad, T., Srivatsava, S., Verma, S., Mo, S. A., & Sahu, N. (2024). Design, synthesis and biological evaluation of imidazole derivatives as analgesic and anti-inflammatory agents. *Scientific Reports, 14*(1), 23121. https://doi.org/10.1038/s41598-024-72399-8
10. Patel, H. M., Bhardwaj, V., Jha, P., Parmar, S. R., Mistry, B., & Patel, P. R. (2021). Structure based design, synthesis, and biological evaluation of imidazole derivatives targeting dihydropteroate synthase enzyme. *Bioorganic & Medicinal Chemistry Letters, 36*, 127819. https://doi.org/10.1016/j.bmcl.2021.127819
11. Pervaiz, S., Mutahir, S., Khan, I. U., Ashraf, M., Liu, X., Tariq, S., Zhou, B.-J., & Khan, M. A. (2020). Solvent-free synthesis of 2,4,5-trisubstituted imidazoles as acetylcholinesterase inhibitors. *Chemistry & Biodiversity, 17*(3), e1900493. https://doi.org/10.1002/cbdv.201900493

12. Rulhania, S., Kumar, S., Nehra, B., Gupta, G., & Monga, V. (2021). An insight into the medicinal perspective of synthetic analogs of imidazole. *Journal of Molecular Structure, 1232*, 129982. https://doi.org/10.1016/j.molstruc.2021.129982
13. Siwach, A., & Verma, P. K. (2021). Synthesis and therapeutic potential of imidazole containing compounds. *BMC Chemistry, 15*(1), 12. https://doi.org/10.1186/s13065-020-00730-1
14. Verma, A., Joshi, S., & Singh, D. (2013). Imidazole: Having versatile biological activities. *Journal of Chemistry, 2013*(1), 329412. https://doi.org/10.1155/2013/329412
15. Yadav, G., & Jain, R. (2025). An insight into synthetic, structural and medicinal perspective of imidazole analogs: A review. *European Journal of Medicinal Chemistry, 290*, 117524. https://doi.org/10.1016/j.ejmech.2025.117524